A LIQUID DIFFRACTION ANALYSIS OF SARCOPLASMIC RETICULUM

I. COMPOSITIONAL VARIATION

G. W. BRADY, D. B. FEIN, M. E. HARDER, AND R. SPEHR, *Division of Laboratories and Research, New York State Department of Health, Albany, New York 12201*

G. MEISSNER, *Department of Biochemistry and Physiology, University of North Carolina at Chapel Hill, Chapel Hill, North Carolina 27514 U.S.A.*

ABSTRACT Intensities of x-ray scattering from a series of fragmented rabbit muscle sarcoplasmic reticulum (SR) samples have been measured over the range $s = 0.05$ to $s = 0.25$. By varying the relative concentrations of lipid and protein (chiefly the Mg^{++}-dependent, Ca^{++}-stimulated ATPase) in the membranes of this series, and by employing methods of analysis appropriate to the scattering from binary liquid mixtures, we have identified the separable contributions of protein and lipid, and the protein-lipid interaction contributions to the total scattering profiles. The shape of the protein term is consistent with scattering from a cylindrical ATPase particle 142 Å in length and 35 Å in diameter. These data imply that the dominant ATPase species is monomeric. The protein-lipid interaction term has been analyzed by a novel treatment based on a determination of the pair correlation function between the electrons of the protein molecule with the electrons of the lipid bilayer in terms of the asymmetry of the transbilayer disposition of the protein. Applied to our results, the analysis indicates a fully asymmetric disposition of ATPase, in which one end of the molecule is contiguous with either the lumenal or cytoplasmic surface of the bilayer.

INTRODUCTION

Sarcoplasmic reticulum (SR) is the membrane vesicular system of muscle which generates intracellular calcium fluxes necessary for myofibrillar contraction and relaxation. The primary catalytic component of active Ca^{++} transport in SR is the Mg^{++}-dependent, Ca^{++}-stimulated ATPase (Ca^{++}-ATPase), a protein which is tightly complexed with phospholipid. Removal of phospholipid from this complex leads to reversible loss of the enzyme's ATP hydrolytic activity (Martonosi, 1969; Meissner and Fleischer, 1972). Furthermore, the kinetic properties of lipid-substituted (Hidalgo et al., 1976; Nakamura, et al., 1976) Ca^{++}-ATPase complexes are sensitive to the physical state of the phospholipid component: an increase in the activation energy of the hydrolysis of a phosphoenzyme intermediate attends the transition to a more immobilized lipid chain structure. In addition, the presence of

---

Dr. Brady is also of the Center for Biological Macromolecules, State University of New York, Albany, New York 12222.

Ca^{++}-ATPase appears to influence lipid structure. Initial results (Hesketh et al., 1976) indicated that Ca^{++}-ATPase protein immobilized stoichiometric amounts of phospholipid chains, although more recent studies showed that this effect is confined to low temperatures (Moore et al., 1978). Because SR exhibits these structurally and functionally significant lipid-protein interactions and because fractions of SR in which CA^{++}-ATPase comprises 90% of the membrane protein may be obtained in large quantities (Meissner, 1975), it is an important and convenient system for studying the role of lipid-protein interactions in the structure and functions of membranes.

To better understand these interactions, ultrastructural and biophysical studies have focused on three salient structural features of SR Ca^{++}-ATPase: the size and shape of the active ATPase molecule, its transbilayer disposition, and its state of self-association. A molecular weight of 115,000 has been determined from sedimentation equilibrium measurements of an ATPase-deoxycholate complex (Le Maire et al., 1976). With regards to ATPase shape, the sedimentation behavior of an active complex of detergent, phospholipid, and monomeric ATPase indicate that the latter is an elongated molecule under these conditions (Le Maire et al., 1976). Electron microscopy has been applied to the determination of ATPase asymmetry and state of association. An alignment of protein favoring the cytoplasmic, or outer, face of SR has been inferred from staining of thin sections of isolated vesicles and of membranes *in situ* (Saito et al., 1978) and from the observed distribution of particles between the two monolayers of freeze-fractured vesicles (Deamer and Baskin, 1969). Stewart and MacLennan (1974) observed that in negatively stained SR vesicles surface particles with a diameter of 30–40 Å are removed by trypsin digestion with a concomitant loss of Ca^{++}-ATPase activity. Using freeze-etching and freeze-fracturing, Scales and Inesi (1976) found that the surface density of protein particles on the cytoplasmic surface of isolated SR vesicles was four times as great as that of the hydrophobic fracture face; a discovery that has been interpreted as indicative of a tetrameric ATPase structure. In this regard, it should be noted that stable, active complexes of ATPase, nonionic detergent, and phospholipid contain a series of polypeptide oligomers (Le Maire et al., 1976; Le Maire et al., 1978).

The analysis of the small-angle scattering from multilamellar assemblies of SR membranes has yielded profiles of the electron density projected along the normal to the membrane surface (Dupont et al., 1973; Liu and Worthington, 1974; Herbette et al., 1978). This technique has not been particularly successful in determining the location of the protein, due among other reasons to the difficulty of reconciling the dynamic distribution of the protein in the membrane with a regular static arrangement as is required for the type of crystal analysis used in the technique. Nevertheless, while disagreeing in the details of the derived profiles (a result of ambiguities in phase determination), all the studies show an asymmetric electron density distribution and the results are rationalized as indicating an asymmetric positioning of the protein across the bilayer, in accord with the ultrastructural studies.

In this paper we present the results of a liquid diffraction analysis of the low angle scattering from suspensions of SR vesicles, with differing lipid-protein concentrations. The diffraction patterns from these systems are liquid-like and are thus well suited to analysis by liquid diffraction techniques (Brady et al., 1979*a* and *b*). These offer the advantage over crystallographic procedures that it is not necessary to draw in a background line as a reference base for phasing the maxima, and thus all the data collected can be used. The data are

analyzed in terms of correlation functions, leading to the separation of the total scattering into its protein and lipid components and to the isolation of the cross correlation term between the electrons in the protein and lipid regions. In this way specific structural information about the different component is obtained as well as the details of how the components are assembled with respect to each other in the membrane. Our analysis thus focused on the determination of the protein shape, its degree of association, and its location in the membrane, with special emphasis on the asymmetry of its transbilayer distribution.

PREPARATION OF SR VESICLES

Membranes were isolated from an intermediate-density vesicle fraction of rabbit skeletal muscle (Meissner, 1975). Membrane vesicles (in 0.3 M sucrose, 0.45 M KCl, 1.5 mM $MgCl_2$, 1 mM EDTA, 10 mM Tris [pH 8.0]) were delipidated with sodium cholate according to method two of Meissner et al. (1973). In the cholate-treated samples, an active Ca^{++}-ATPase accounted for 90–95% of the protein (Moore, et al., 1978). Different amounts of sodium cholate (2–5 mg/ml) were added to vesicle suspensions (4.5 mg protein/ml) to obtain the desired range of phospholipid removal. The partially delipidated vesicles were recovered by centrifugation for 2 h at 127,000 × *g*. Pellets were resuspended in a Potter-Elvehjem hand homogenizer in 0.3 M sucrose, 50 mM KCl, 1 mM HEPES (pH 7.5), and dialyzed against several changes of the same buffer for 24 h. Membranes were finally transferred into a medium of low electron density by centrifuging and resuspending samples three times in 1 mM KCl, 1 mM HEPES (pH 7.4). Membranes (20–50 mg protein/ml) were stored at −65°C before use. One series of delipidated vesicles was prepared with [^{3}H]cholate (~10^6 cpm/mg of cholate) and analyzed to confirm that >99% of the detergent was removed from the vesicle preparations by the above procedure.

A control SR sample was obtained by washing the intermediate-density vesicle fraction three times with 1 mM KCl, 1 mM HEPES (pH 7.4). We wish to emphasize that cholate-treated SR vesicles were comparable to the control vesicles in two respects. First, the specific activities of Ca^{++}-ATPase in the two samples were comparable (Moore, et al., 1978). And second, within the limits of experimental error, the scattering curve of untreated

TABLE I
PROTEIN AND LIPID CONCENTRATIONS AND VOLUME FRACTION OF PROTEIN

Sample	Concentration		Volume fraction protein
	Protein	Lipid	
	(mg/ml)		
1	24	13.6	0.36
2	34	18.2	0.59
3	37.5	18.2	0.61
4	37	14.2	0.66
5	47	13.6	0.72
6	45	11.7	0.74

Protein and lipid concentrations were measured as described in the text. The volume fraction of proteins was calculated using values of 0.740 and 0.975 for the partial specific volumes of protein and lipid, respectively.

membranes was identical to that of cholate-treated membranes of similar protein concentration and protein-lipid ratio (open circles in Fig. 1).

Protein content of partially delipidated membranes was estimated by the procedure of Lowry et al. (1951) using bovine serum albumin as a standard. Total phosphorus was measured as an estimate of lipid phosphorus (Meissner and Fleischer, 1971) using a modification (Rouser and Fleischer, 1967) of the method of Chen et al. (1956).

Volume ratios of protein and phospholipid were calculated using molecular weights of 115,000 and 800 for the Ca^{++}-ATPase and phospholipid, respectively. Partial specific volumes were 0.740 and 0.975 for protein and phospholipid, respectively (Le Maire et al., 1976*b*). Protein and lipid concentrations and volume fractions in the samples are shown in Table I.

DATA COLLECTION AND PROCESSING

The data were taken with a position sensitive detector. A sample to detector distance of 50 cm was used for most of the measurements, but the data at the lowest angles was rechecked by increasing this distance to 100 cm. The main beam (CuK α radiation, λ = 1.54 Å) was collimated by two pinholes 0.75 mm in diameter, separated by 50 cm. 120 channels were used, covering the scattering range between $s = 0.03$ and $s = 0.44$ ($s = (4\pi/\lambda) \sin \theta$, where λ is the wavelength and θ is one-half the scattering angle). The temperature was 21°C. The data were collected in an 11/03 DEC Microprocessor (Digital Equipment Corp., Maynard, Mass.), and after the run was terminated they were transferred on command to a PDP 8/E minicomputer (Digital Equipment Corp.), where they were averaged over a five-channel interval by a least squares program. The patterns were corrected for background by subtracting the scattering of the cell filled with buffer. Each step could be monitored by a printout or an oscilloscope display. The samples were contained in a cell fitted with 1-mil mica windows and had a thickness of 1 mm. Absorption corrections were negligible. No deterioration or settling of the sample was observed, as demonstrated by a constant counting rate at all scattering angles during the course of each experiment. The apparatus was monitored repeatedly by measuring the intensities and positions of the reflections from a lead stearate sample and these varied by <2%.

Fourier transforms were evaluated by computer integration of the equation:

$$I(s) = \int_0^\infty D_{jk}(r) \frac{\sin sr}{sr} \, dr,$$

where $D_{jk}(r)$ is the sum of the electron pair distributions for each type of interaction, with $j = k$, $j \neq k$, and $I(s)$ is the measured intensity, corrected for background and absorption. A fast Fourier transform or Simpson's rule algorithm was used for the integration. With the number of experimental points used, the error was <1%.

Scattering profiles from cylinders of varying (see Discussion) axial ratios were computed using the formula (Guinier and Fournet, 1955):

$$I(s) = \int_0^{\pi/2} \frac{\sin^2(sH \cos \theta)}{s^2 H^2 \cos^2 \theta} \times \frac{4 J_1^2(sR \sin \theta)}{s^2 R^2 \sin^2 \theta} \sin \theta \, d\theta,$$

where H and R are the half height and cylinder radius, respectively. Scattering profiles for ellipsoids of revolution were taken from published tables (Guinier and Fournet, 1955; Beeman et al., 1957).

The calculation of the protein-lipid correlation term is presented in the Appendix. This calculation was too lengthy for the PDP8/E and was evaluated numerically using a PDP 11/45 computer.

THEORY

The amplitude scattered in a direction defined by a unit vector $\mathbf{h}$ from a point P_j of electron density ρ_j in a stationary particle or aggregate is given by the expression:

$$A_L = \rho_j e^{-(2\pi i/\lambda)(\mathbf{h}-\mathbf{h}_0)\cdot\mathbf{OP}_j},$$

where λ is the wavelength of the radiation (CuKα = 1.54 Å), $\mathbf{OP}_j$ is the distance vector of the point from an arbitrary origin 0, and $\mathbf{h}_0$ is a unit vector along the direction of the main beam. We designate the vector $(2\pi/\lambda)\,(\mathbf{h}-\mathbf{h}_0)$ as $\mathbf{s}$; its magnitude is $(4\pi/\lambda)\sin\theta$, where θ is one-half the scattering angle. The total amplitude scattered by the aggregate is obtained by summing over all the points in it. Thus

$$A(s) = \sum_j \rho_j e^{-i\mathbf{s}\cdot\mathbf{OP}_j}. \tag{1}$$

The intensity is obtained by multiplying A by its complex conjugate, with the result that

$$\begin{aligned} I(s) &= \sum_j \sum_k \rho_j \rho_k \cos\,(s \cdot \mathbf{P_j P_k}) \\ &= \sum_j \sum_k \rho_j \rho_k \cos\,(s \cdot \mathbf{r_{jk}}). \end{aligned} \tag{2}$$

Our system is a suspension of membrane vesicles. These are in thermal motion. Translation has no effect on the intensity expression, but rotations do, and Eq. 2 must be averaged over all orientations in space. This can be done rigorously by expanding Eq. 1 in spherical harmonics (Stuhrmann, 1973; Brady et al., 1977). We follow here the simpler treatment given by Guinier (1955), based on averaging the function $\cos\,(\mathbf{s}\cdot\mathbf{r})$ as the vector $\mathbf{r}$ takes up all orientations in space with equal probability. This is equivalent to multiplying $\cos\,(\mathbf{s}\cdot\mathbf{r})$ by $1/2\sin\alpha\,d\alpha$, the probability that the angle α between the vectors $\mathbf{r}$ and $\mathbf{s}$ lies between α and $\alpha + d\alpha$, then integrating between the limits 0 and π. Then:

$$\begin{aligned} \overline{\cos\,(\mathbf{s}\cdot\mathbf{r})} &= \int_0^{\pi} \cos\,(sr\cos\alpha)\,\frac{\sin\alpha}{2}\,d\alpha \\ &= -\frac{1}{sr}\int_0^{\pi/2} \cos\,(sr\cos\alpha)\,d\,(sr\cos\alpha) \\ &= \frac{\sin sr}{sr}, \end{aligned}$$

which when inserted in Eq. 2 gives the Debye expression for the intensity:

$$I(s) = \sum_j \sum_k \rho_j \rho_k \frac{\sin sr_{jk}}{sr_{jk}}. \tag{3}$$

This brief derivation of the Debye equation serves to illustrate that an essential requirement is that the system to which it is applied be randomly oriented. Thus it cannot be used on membrane systems made up of stacked or otherwise oriented bilayers or multilayers. Further, the intensity is expressed as the double sum of the function $\sin sr_{jk}/sr_{jk}$ over all distances r_{jk} between pairs of points j and k, each term being weighted by the product of the electron densities at the points j and k. This summing over pairs of points implies that the system exhibits short range order (which can be quite specific and detailed), but no long range order, that is, that the structure cannot be visualized as a regular repeating unit, where amplitudes scattered from planes are added, and where the scattering is essentially given by a lattice function sampling the bilayer (unit cell) scattering only at values of s corresponding to a multilayer repeat. Liquids are typical of systems which exhibit short range order only. The components are in constant motion, but on the average the resultant structure shows a grouping around certain preferred distances. When all the distances are measured and the double sum taken, these preferred distances are sufficient to produce maxima in the resulting continuous intensity patterns. The magnitude and definition of these maxima (and minima) is, of course, determined by the amount of order present. Membranes, consistent with the modern view of them as being essentially solutions of protein and lipid, show diffraction patterns of just this kind, and therefore it is appropriate to use liquid diffraction methods in their analysis. Also, the terms in the summation can be conveniently grouped into those over all point pairs in the protein, all point pairs in the lipid region, and all point pairs in which the two points are not in the same component. We then write that

$$I(s) = \left(\sum_j \sum_k \rho_j \rho_k \frac{\sin sr_{jk}}{sr_{jk}}\right)_p + \left(\sum_l \sum_m \rho_l \rho_m \frac{\sin sr_{lm}}{sr_{lm}}\right)_l + \left(\sum_n \sum_o \rho_n \rho_o \frac{\sin sr_{no}}{sr_{no}}\right)_{pl} = I_p + I_l + I_{pl} \tag{4}$$

$$NI_{uc} = N(xI_p^0 + (1 - x)\, I_l^0 + 2x\,(1 - x)\, I_{pl}^0 \tag{5}$$

where I_{uc} is the scattering of a unit of composition, x and $(1 - x)$ are the mole fractions of protein and lipid in the unit of composition and I_p^0 and I_l^0 are the scattering per mole of protein and lipid, respectively. For the protein we chose the molecule itself as the basic scattering unit, and for the lipid "mole" we chose a hypothetical aggregate of lipid molecules large enough to constitute a lipid bilayer phase, and thus to exhibit a scattering pattern characteristic of the bilayer structure. For the present study, the actual units in which the composition and concentration are expressed is not critical since, as will be seen, the protein component of the scattering can be identified directly from its concentration dependence (in mg/ml), and the lipid scattering term will only be discussed qualitatively. But the analysis is very much in the spirit of Eqs. 4 and 5, and presented in this form the equations serve to highlight the fact,

previously stated, that the scattering can be expressed in terms of the scattering from the individual components, and that manipulation of the protein-lipid ratio constitutes a powerful tool for isolating these different scattering terms.

Small angle scattering is not sensitive to fluctuations on an atomic scale so the electron densities can be considered as continuous functions. Eq. 5 can then be written in integral form:

$$I(s) = \int_V \int_V \rho_j \rho_k \frac{\sin sr_{jk}}{sr_{jk}} \, dV_j \, dV_k, \tag{6}$$

where the double integration is over the volume of the aggregate. In membranes there are three regions of different electron density: the protein molecule with electron density ρ_1, the polar head group region of the lipid bilayer with electron density ρ_2, and the interior hydrocarbon region with electron density ρ_3. Each of these regions can be characterized by a density distribution function $D(r) = 4\pi r^2 \rho^2 C(r)$, where $C(r)$ is defined as the probability of finding another electron at a distance between r and $r + dr$ from each electron in that region. The quantity $D(r)\,dr$ is thus the number of electron pairs with a separation between r and $r + dr$ in that region. The scattering from the three regions can then be written in terms of the three distribution function as the sum:

$$I_p + I_l = \int_0^\infty D_{11}(r) \frac{\sin sr}{sr} dr + \int_0^\infty D_{22} \frac{\sin sr}{sr} dr + \int_0^\infty D_{33} \frac{\sin sr}{sr} dr.$$

The rest of the scattering, given by the cross-correlation term I_{pl}, will also contain three terms characterized by the function D_{12}, D_{13}, and D_{23}, signifying correlations between the electrons in the respective regions denoted by the subscripts. As before, each integral is weighted by a concentration term. It is customary to use volume fractions when the scattering is formulated in terms of the $D(r)$s as in Eq. 6, but to be consistent we can retain the mole fraction notation of Eq. 5. The important thing for our purposes is that the protein scattering be expressed in units which relate it to the scattering per protein molecule.

The equations given above are for a sample *in vacuo*. For a sample suspended in a solvent, they must be modified to take account of the presence of the latter. The solvent is equivalent for scattering purposes to a fluctuation of uniform density ρ_0 which permeates the whole irradiated volume; its continuity is not seriously perturbed by the much shorter range fluctuations ρ_1, ρ_2, and ρ_3. These latter are thus considered to be superimposed on this long range fluctuation ρ_0. Thus at each point i, where due to the presence of the aggregate there exist fluctuations ρ_1, ρ_2, and ρ_3, the values of the corresponding densities are $\rho_1 + \rho_0$, $\rho_2 + \rho_0$ and $\rho_3 + \rho_0$, respectively. Thus the solvent density must be subtracted from the density at each point i to obtain the values of ρ_1, ρ_2, and ρ_3, which are, of course, the ones effective in producing the diffraction pattern of the suspended membrane aggregate. We thus have at a point i where a fluctuation ρ_1 is present:

$$\rho_1 = \rho_i - \rho_0 = (\rho_1 + \rho_0) - \rho_0 = (\rho_1 - \rho_0) + \rho_0,$$

with similar expression for ρ_2 and ρ_3. Substituting for ρ_1 in the term containing D_{11}, we have

$$I_{11} = \int_0^\infty D_{11}(r) \frac{\sin sr}{sr} \mathrm{d}r$$

$$= \int_0^\infty (\rho_1 - \rho_0)^2 C_{11}(r) \frac{\sin sr}{sr} 4\pi r^2 \mathrm{d}r + \int_V^\infty \rho_0^2 C_{00}(r) \frac{\sin sr}{sr} 4\pi r^2 \mathrm{d}r$$

$$+ 2 \int_0^\infty \rho_1 \rho_0 C_{10}(r) \frac{\sin sr}{sr} 4\pi r^2 \mathrm{d}r. \tag{7}$$

The second term above corresponds to the scattering from the total volume V_0 with uniform density ρ_0. For an irradiated volume of ~ 1 mm^3 the contribution from this term is present only at immeasurably small angles. The third term is similarly unobservable, since $C_{10}(r)$ is unity for all values of r (since ρ_0 is continuous), and this term is again an integration of $\sin sr/sr$ over the volume V_0. We have finally that

$$I = \sum_{i,j=1}^{3} \int D_{ij}(r) \frac{\sin sr}{sr} \mathrm{d}r$$

$$= \sum_{i,j=1}^{3} \int (\rho_i - \rho_0)(\rho_j - \rho_0) C_{ij}(r) \frac{\sin sr}{sr} 4\pi r^2 \mathrm{d}r. \tag{8}$$

It should be underlined that the last two terms involving ρ_0 in Eq. 7 are not to be confused with the scattering observed at the lower angles from protein-containing membranes, or with the zero-angle value of the intensity obtained by extrapolating these observed values to zero-angle. The long-range ρ_0 terms are confined to angles corresponding to values of $s < (2\pi/\mathbf{R}) \approx 10^{-6}$, where $\mathbf{R}$ is an average dimension of the irradiated volume. They are thus not considered to belong to the domain of observable small-angle scattering. Thus the presence of the solvent is only manifested through its effect on the densities ρ_i and ρ_j, which as shown in Eq. 8, is to cause them to be replaced by their effective values $\rho_i - \rho_0$ and $\rho_j - \rho_0$, respectively. Nor should the ρ_0 terms be confused with the background scattering observed when the cell is filled with solvent only. This latter is largely due to extraneous scattering from the slit system. In some cases, for example when sucrose solutions are used as the suspending medium, there is indeed measurable added scattering from the solvent. This results from the presence of the large sucrose molecules which manifest themselves as density fluctuations of a range long enough to produce small-angle scattering, and which are themselves superimposed on the ρ_0 fluctuations. Pure H_2O, on the contrary, exhibits no observable scattering. This scattering (from the sucrose) is, of course, removed when the background is subtracted.

Eq. 8 is the basis for a second method, in which varying the solvent electron density is used as a tool for analyzing the scattering, and the next paper in this series will present the results of its application to the SR membrane. There, instead of varying the lipid-protein ratio, the diffraction pattern is measured at different values of ρ_0. The contribution of each term in Eq. 8 is thus modulated by the respective increase or decrease of $(\rho_i - \rho_0)$ $(\rho_j - \rho_0)$ of that term (an obvious case is when ρ_i or $\rho_j = \rho_0$; the term then vanishes). The intensity is then expressed as a set of linear equations with independent coefficients, which can be solved for the respective

C_{ij}s. The application of this technique to a membrane containing myelin protein has been described (Brady et al., 1979*b*).

The application of Eq. 8 to the present system is concerned primarily with the isolation and analysis of the protein and protein-lipid terms of Eq. 8. The details of the isolation procedure are described in the next section. For the analysis of the protein scattering, since the volume of the ATPase monomer was known from other data, combinations of radii of gyration and axial ratios were chosen to characterize the molecule. The scattering pattern for each such combination was calculated, and the result compared to the experimental data. A unique combination, determining both the shape of the enzyme and its degree of polymerization was found to fit the data.

The relative asymmetry of the placement of the protein in the bilayer was also determined by comparing model intensities with experimental ones. Here, using methods described in the Appendix, density distribution functions were evaluated for a model which is consistent with the results of the determination of the protein and lipid structure (see Results). The density distribution $D_{1,23}$ actually calculated was that between the electrons of the protein and electrons of both the polar head group and hydrocarbon interior electrons, that is $D_{1,23} = D_{12} + D_{13}$. The model consists of a protein cylinder orthogonal to an annular lipid bilayer and inserted through the bilayer with a variable degree of asymmetry (in case of minimum asymmetry, the cylinder ends are equidistant from the bilayer center; in the case of maximum asymmetry, one end of the cylinder is contiguous with one surface of the bilayer). The electron density of the bilayer is approximated by a symmetric step function. An outer boundary to the lipid annulus around each protein is estimated to take account of the dampening effect on the density distribution function of the loss of long range order in the liquid-crystalline lipid, brought about by thermal motion, variations in curvature, and the disrupting effect on the bilayer structure resulting from the presence of the other protein molecules randomly distributed in the bilayer. Substituting the model $D_{1,23}(r)$ functions in the lipid-protein terms in Eq. 8 yields corresponding intensity functions. The positions of the maxima in these functions depend on the dimensions of the protein and the asymmetry of its transbilayer disposition, but is relatively insensitive to the width of the lipid bilayer or to the relative volumes (and number of electrons) in the hydrocarbon and polar regions of the bilayer. Therefore, we can determine the asymmetry of the protein placement from a comparison of observed and calculated protein-lipid interaction terms provided the dimensions of the protein are known.

An alternative procedure is to use the isolated components of the scattering in Eq. 8 to obtain directly the respective $D_{ij}(r)$s by Fourier transformation of the measured data. Thus

$$\frac{D_{ij}(r)}{r} = \frac{2}{\pi}\int_0^\infty s\, I_{ij}(s) \sin sr \, dr.$$

This procedure is particularly useful for centrosymmetric structures, such as a symmetric lipid bilayer, where $D'_{ij} = D_{22} + D_{33}$ is identified with the convolution square of the electron density distribution; it may therefore be deconvoluted (Pape et al., 1974) to obtain the electron density profile of the bilayer. Since, for reasons stated subsequently, the lipid-protein

ratios used in this study were less than ideal for a quantitative analysis of the lipid contribution, we have postponed this phase of the study until later.

RESULTS AND DISCUSSION

The scattering curves for the SR membrane at six different protein to lipid ratios were determined. Since the protein and lipid concentrations of the six samples fell into three distinct sets, as indicateed in Fig. 1, the curves in each set were averaged, giving three scattering curves representative of three widely differing protein concentrations; these are the curves plotted in the figure. The data covers the range from $s \simeq 0.05$ out to $s \simeq 0.22$. The scattering at values of $s \gg 0.22$ is very faint and no special attempt was made to accurately measure the intensities beyond this value. The scattering in this higher angle range (beyond $s \simeq 0.22$) is virtually all from the lipid component (Brady et al., 1979; Wilkins et al., 1971) and the obvious way to improve the accuracy is to increase the lipid concentration. On the other hand, as stated in the Introduction, the primary aim of our work was the identification and analysis of the protein and the protein-lipid components of the scattering. For this purpose, the protein concentration, and thus the protein/lipid concentration ratio, had to be kept as high as possible. Because of solubility considerations, this had to be done at the expense of the lipid concentration, with a consequent decrease in the contribution of the lipid

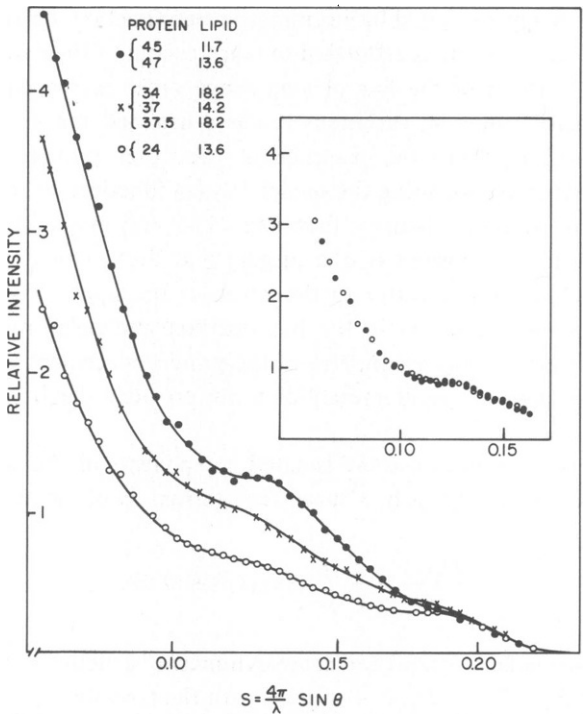

FIGURE 1 Measured scattering curves for SR membranes of protein/lipid ratios. The compositions are listed in the figure. The inset shows the scattering curve of the highest concentration sample (●) scaled to that of the lowest concentration (O) by dividing by the ratio of the protein concentration.

term to the total intensity. We thus content ourselves in this work with a semiquantitative evaluation of the lipid term, since it does not influence the rigor with which our primary objectives can be attained.

As Fig. 1 shows, all the curves exhibit a marked increase in scattering at the lowest angles. This inner scattering increases with the protein concentration. In membrane systems which do not contain protein, the scattering decreases to zero in this region (Brady et al., 1979*a*; 1979*b*; Wilkins et al., 1971). This fact allows the isolation of the protein dependent part of the scattering from that arising from the lipid.

The next notable feature of the curves is the presence of a peak whose maximum is centered at $s \simeq 0.13$. Its magnitude also increases with the protein concentration. In fact, a further striking property of the curves is that when scaled to the same protein concentration, both the inner and intermediate regions superimpose within experimental error, deviating from each other only at values of $s \gg 0.16$. This is the behavior predicted by Eq. 3b for the protein and protein-lipid terms. The scaling is shown in the insert where the averaged curve for the highest protein concentration (46%) has been scaled to that of the lowest protein curve (24%). (The curve for the intermediate concentration also scales in the same manner.) Thus the intensities out to $s = 0.16$ are directly proportional to the protein, and equally significant, increasing the proportion of protein in the membranes does not change the shape of the curves.

Finally, beyond $s \simeq 0.16$, all the curves show the presence of a peak, centered at $s = 0.185$, which appears as a shoulder on the curves. This value of s corresponds to a distance of 41.3 Å, which we can tentatively identify with the phospholipid bilayer thickness. This assessment is supported by the fact that the intensity of this peak is proportional (within the previously stated experimental limitations) to the lipid concentration. Thus the intermediate curve, with the highest lipid concentration, is more intense than the curves for the other two concentrations. We will return to a discussion of this region later.

Proceeding to a quantitative evaluation of these curve features, we start first with the inner scattering. This type of scattering, concentrated around the zero angle and decreasing with increasing angle, is identified in liquid systems as arising from an extended region of scattering matter of constant electron density, and the invariance of the shape of the scattering curve with concentration is consistent only with an increase in the number of such regions. A protein molecule, either single or associated into a polymeric form, can be identified with such a region, and the observed protein concentration dependence is then seen to result from an increase in the number of such protein molecules. Since the scattering curve of such a particle will be determined at the low angle end by its size, as measured by a parameter such as the radius of gyration, and at the higher angle end by its shape (Guinier, 1955), we can use this inner pattern to characterize the protein dimensions. The procedure used is illustrated in Fig. 2. The experimental points are plotted as open circles. Calculated scattering curves for various sizes and shapes appear as solid lines. The curves designated by $V = 1$ are single protein molecules of volume 1.41×10^5 Å^3. Their shape is denoted by the ratio, H/R, of their half-height to their radius, assuming a cylindrical shape for the molecule (curves for ellipsoids of revolution with the same axial ratio do not differ significantly from the cylinder curves). These curves were scaled to the experimental curve at $s = 0.058$, a point chosen as representative of the region where the curves are determined by the radius of gyration. Also shown are curves for $V = 4$, a cylindrical aggregate of four protein molecules,

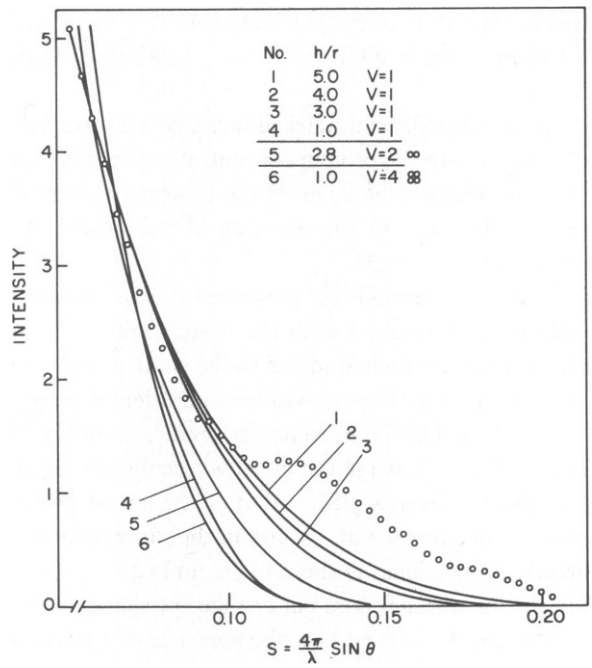

FIGURE 2 Calculated scattering curves for protein entities of different volumes and shapes. $V = 1$ denotes a single nonassociated protein molecule. The calculated curves have been normalized to the measured curve at $s = 0.058$, except the curve for $V = 4$, where the normalization was done at $s = 0.062$ to better display its deviation from the measured curve at the low angles.

postulated by Scales and Inesi (1976) to explain their electron microscope results, and an aggregate designated by $V = 2$, consisting of two proteins stacked side by side. Other axial ratios and sizes were, of course, calculated and tested, but none fitted the data better than those shown here. Since they added nothing to the interpretation and their inclusion would needlessly clutter the graph, they were not plotted.

Two of these cases can be eliminated at once. The scattering curve for the tetrameric aggregate ($V = 4$) has a much higher slope than the experimental curve at the lowest angles and deviates markedly from it with decreasing scattering angle. Also, its intensity becomes negligible beyond $s \simeq 0.12$, and the observed protein dependence between $s \simeq 0.12$ and $s \simeq 0.16$ would not be accounted for. The curve for the single protein molecule with unit axial ratio ($V = 1$, $H/R = 1$) can be eliminated for this latter reason also, even if it gives a reasonably good fit at the lower angles. (The fact that a large part of the protein dependence right out to $s \simeq 0.16$ has to be included in the protein scattering curve should be intuitively evident at this point from the general character of the measured curves, and will be seen to be an essential requirement in the subsequent analysis of the protein-lipid interaction term.)

The two models eliminated above, although differing in all other respects, possess the same unit axial ratio, and indicate that the data cannot be reconciled with proteins having such symmetrical shapes. This is confirmed by the characteristics of curves 1, 2, and 3, calculated for single protein particles with axial ratios of 3, 4, and 5. These three curves coincide exactly with the experimental ones at the low angles and the outer angle tails extend out to cover the

whole scattering range, over which the measured curves show the protein concentration dependence. Axial ratios >5 show high angle tails extending out beyond the range of observable scattering; in fact the tail of the curve with axial ratio 5 extends well beyond $s \simeq 0.16$ and is still significant in the region of the curve where the protein dependence no longer applies. As opposed to this, an axial ratio of 3 generates a tail which fades out too quickly. Thus, although at this stage of the analysis curves 1, 2, and 3 could all be said to give reasonable fits, curve 2, for the above reasons, gives the best agreement with the data. This corresponds to the scattering from a single symmetrical protein particle of volume 1.41×10^5 $Å^3$ with a radius of 17.7 and a half-height of 71 Å.

The finding from the isolated protein scattering analysis that the protein exists as single particles does not, of course, rule out the presence of higher oligomeric forms. This is shown in Fig. 3, where, as an example, the curve calculated for the scattering in a system of 100 particles in which 15 are in dimeric form and five in tetrameric form is compared with the curve in which the 100 particles are in monomeric form. It is seen that in the observable scattering range the curves are compatible. This results because the differences in scattering of the higher forms are concentrated primarily at the very small angles, and are thus not readily detectable in the scattering range shown in the figure. When the proportion of polymeric forms increases much beyond this amount, the differences become marked, however. Thus as a rough limit it could be stated that a significant number, $\leq 20\%$, of the proteins could be associated. The presence of these oligomers is to be expected at the high protein concentrations found in these membranes, and the equilibrium between high and low forms offer another mechanism for biological activity, as well as being compatible with the evidence from freeze-fracture studies that at the drastically lowered temperatures used in those studies the equilibrium is shifted toward the higher forms.

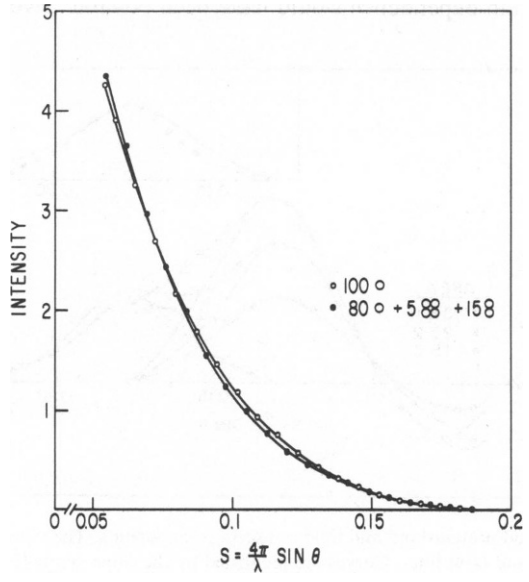

FIGURE 3 Comparison of a calculated protein scattering curve for 100 single particles with one calculated for the same number of particles but in which 20 are in dimeric and tetrameric form.

This protein component is the contribution of the first term in Eq. 5. When subtracted from the measured curves, the remaining two terms of Eq. 5 are then isolated. These are shown in Fig. 4 for the three sets of membrane samples listed in Fig. 1. The difference pattern shows two sets of slightly overlapping peaks which can easily be resolved from each other. The first set, with maximum at $s = 0.132$ is protein dependent. The second set, with maximum at $s = 0.178$, as briefly discussed earlier, is protein independent. This identifies it with the second term of Eq. 5, the lipid term, whose coefficient depends only on the lipid concentration. This assignment receives additional support by comparing it to the pattern for single bilayers of egg lecithin determined by Wilkins et al. (1971), shown in the insert of Fig. 4. The curves are very similar, and while it is not quite rigorous to assume that the lecithin is a prototype of all lipid bilayers, most free lipid patterns resemble each other in their gross features, and the comparison is justified in the semiquantitative sense that we are treating the lipid component of the scattering. This leaves only the protein dependent region of Fig. 4 to be accounted for and it must then correspond to the protein-lipid term of Eq. 3b. The areas under the curves, listed in the figure, are in the ratios 1:1.52:2.1, to be compared to the ratios of the protein concentrations, 1:1.46:1.91.

The fact that the areas of the peaks at $s = 0.132$ are (also) directly proportional to the protein concentrations, strengthens the correctness of the choice of curve 2 in Fig. 2 as properly describing the independent protein scattering. Further, since the protein-dependent region (out to $s = 0.16$) has been shown to be made up of two terms, it would be virtually impossible to deduce a consistent explanation for the protein dependence, given the nature of the protein scattering curves, without invoking the same concentration dependence for both terms throughout the region. If, for example, curve 4 had been chosen to represent the protein scattering, the intensities, positions, and shapes of the resultant difference curves would have changed drastically from curve to curve in Fig. 1 in a manner such that no rational explanation of the protein dependence would have been possible. Even curve 3, characterized

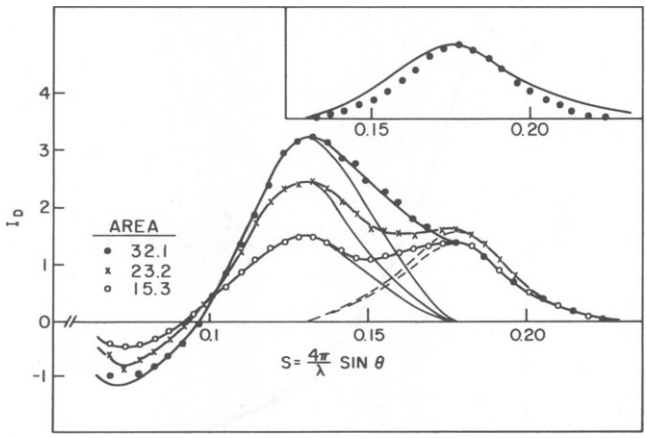

FIGURE 4 The isolated protein-lipid and lipid scattering components. The two can easily be resolved, as shown by the dashed and faint lines. Curves are identified by the same symbols used in Fig. 1. The insert shows the resolved lipid portion of the scattering curve compared to the data of Wilkins et al. (29) for egg lecithin bilayers, after approximate desmearing to match our geometrical conditions.

previously as defining the lowest possible value of H/R for which an acceptable fit could be rationalized, would have led to an unsatisfactory smearing of the left hand side of the difference pattern. Conversely, if the analysis had been initiated by considering first the set of peaks at $s = 0.132$, and a protein dependence different from that found above for the independent protein scattering had been invoked, a consistent interpretation of the inner portion of the scattering curves would have been impossible.

The protein-lipid term is given by

$$I_{pl} = 2x(1 - x) \int_0^\infty D_{1,23}(r) \frac{\sin sr}{sr} \, dr. \tag{9}$$

The electron pair function $D_{1,23}(r)$ is the sum of distances, measured from each electron in the protein to all the electrons in the lipid, and vice versa, and depends on the location of the protein with respect to the lipid phase of the membrane. The Ca^{++}-ATPase in SR is internally placed in the bilayer, as shown by freeze-fracture electron micrographs, penetrating at least partially into the interior, and to determine its most probable location it is necessary to calculate appropriate $D(r)$s for different degrees of penetration, evaluate the Fourier transforms for each $D(r)$ and compare the result with the isolated protein-lipid term in Fig. 3. The details of the calculation are described in the Appendix. The model chosen, shown in Fig. A1, has the protein oriented with its long axis perpendicular to the bilayer plane. For computational convenience, the boundaries between the positive and negative electron density regions of the lipid have been squared off, and the distance between the midpoints of the two positive regions is set equal to 41.8 Å, the measured bilayer spacing. (Rounding off the boundary regions does not significantly affect the results.) Appropriate $D(r)$s were calculated for three positions of the protein with respect to the bilayer: symmetrically placed with equal portions extending out on either side of the bilayer; one end of the protein contiguous with one face of the bilayer, and the other end protruding out from the bilayer; a position midway between these two. The appropriate integrals were evaluated on an 11/45 computer. The $D_{1,23}(r)$ curve for the second case is shown in Fig. 5. As drawn, the curve is for an ordered layer extending out indefinitely, and does not take into account the dynamic liquid nature of the system, with attendant disappearance of long range order. To rectify this, a quantity ρ_0 is introduced and a function $D'_{1,23}(r)$ defined by the relation:

$$D'_{1,23}(r) = D_{1,23}(r) - 4\pi r^2 \rho_0^2,$$

is used instead of $D_{1,23}(r)$. A value of ρ_0 is then chosen such that at large r, $D'_{1,23}(r) \rightarrow 0$. In terms of the intensity this implies that at the small angles corresponding to these large distances the intensities, given by

$$I_{1,23} = \int_0^\infty D'_{1,23}(r) \frac{\sin sr}{sr} \, dr$$

reduce to

$$I_{1,23} = \int_0^\infty D'_{1,23}(r) \, dr,$$

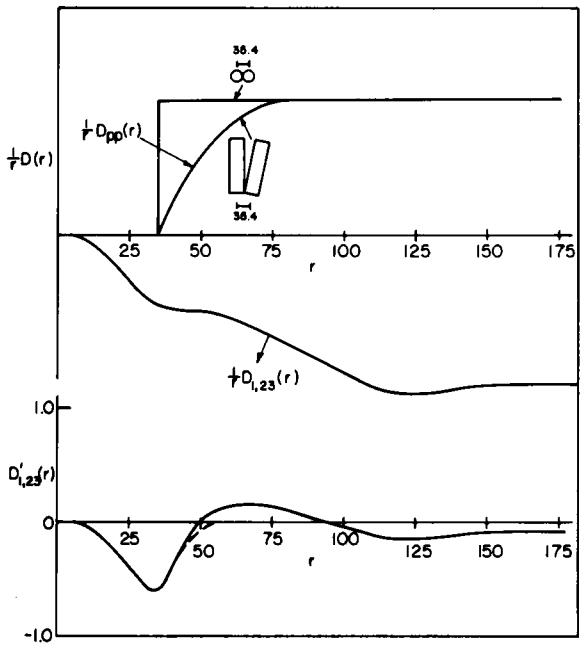

FIGURE 5 Calculated $D_{12}(r)$ curves for the most asymmetrically placed protein. Also shown are interparticle protein electron correlation curves, $D_{pp}(r)$. As explained in the text, these latter are effective in limiting the range of $D(r)$ to the first ~50 Å of the bilayer. The resultant $D'_{12}(r)$ is shown in the lower part of the graph.

and thus also tends toward zero. The quantity ρ_0^2 is related to the mean value of the product of the electron density fluctuations in the system and reflects the fact that at large distances preferred distances and orientations become random, with the result that positive and negative fluctuations superimpose and thus cancel out. In the case considered here, the bilayer would have its continuity disrupted by the presence of other proteins randomly distributed in the bilayer, by local fluctuations in curvature and thickness, and by other disordering affects brought about by the diffusional motion of both the proteins and lipid molecules. The consequence of this is that beyond a certain distance from each protein there is no further correlation of the lipid structure with the protein. The most important of these disordering effects is the presence of other proteins, and a semiquantitative consideration of it is worthwhile in showing how the lipid-protein interaction is determined by the first few layers of lipid around the protein. The interaction of each protein particle with the other proteins in the system is expressed by correlation terms between the electrons in different particles. These terms are positive, since they are between effective electron densities of like sign, as opposed to negative protein-lipid terms which result from the correlation between positive protein electron densities and a net negative effective electron density of the phospholipid. Consequently, if a protein lipid-component is present at the same value of r as a protein-protein component, the two counteract, and the net correlation at this value of r is the difference between the two. The correlation function for randomly distributed particles is difficult to calculate except for spherical particles (Guinier, 1955), since the effect on the functions of

mutual misorientation of the long axes of the proteins with respect to each other cannot be properly accounted for at the present stage of our knowledge of the structure. However, it is not necessary to do this to arrive at a valid estimate of the range of the lipid-protein correlation. By definition, a random distribution (of protein) is one in which a particle can take up any position in the bilayer except that occupied by another particle. The corresponding correlation function for a random planar distribution of spherical particles of radius 17.7 Å is also shown in Fig. 5. The probability of finding another particle is zero at distances <35.5 Å (=$2R$) and unity at distances >$2R$. For cylindrical proteins, slight misorientations would dampen the instantaneous rise of $C(r)$ to unity at $r = 2R$, since all the electrons would not be at the same mean distance apart. These misorientations result not only from slight variations from the normal in the orientation of the protein relative to the bilayer, but also from changes in orientation of one area of the bilayer with respect to another. This is illustrated graphically in Fig. 5 where two proteins are shown placed at a distance of closest approach =$2R$, but with their long axes oriented at an angle of 10° to each other. (This is certainly a reasonable estimate of the degree of misorientation.) Under these conditions, instead of rising sharply, $D_{pp}(r)$ for the protein-protein interaction only attains its full value at $r \simeq 80$ Å. An estimate of the magnitude of $D_{pp}(r)$ relative to $D_{1,23}(r)$ can be obtained from the composition, molar volumes, and effective densities of the constituents. The electron densities (in $el/Å^3$) for the protein, the interior hydrocarbon region, and the polar head group region are 0.402, 0.270, and 0.380, respectively, and with reference to a solvent electron density of 0.335 give 0.067, −0.065, and 0.045 for the corresponding effective electron densities ρ_P, ρ_L^-, and ρ_L^+. For the intermediate concentration (36 mg/ml protein; 16.9 mg/ml lipid), dividing by the molecular weights leads to a number ratio of 134.6 lipid molecules/2 protein molecules. When converted to volumes, and including a packing factor of 1.1 to take account of the hexagonal stacking of the lipids, this leads to volume fractions $\overline{V}_2$ and $\overline{V}_1$ of 0.456 and 0.544 for the lipid and protein, respectively. Finally, we need to know the probability P of an element of electron density in a protein particle being correlated with an element of electron density in another protein relative to the probability of its being correlated with an element of electron density in the lipid. This is obviously given by the ratio of the total volumes of protein and lipid extrinsic to the origin protein particle in the planar membrane, that is, the ratio of one protein volume to 133 lipid volumes, or $P = [(1.40 \times 10^5)/(2.56 \times 10^5)] = 0.55$. We can then write for the protein-protein correlation, that $D_{pp}(r) = P\overline{V}_1^2\rho_P^2$. At the larger distances (>150 Å) where the scaling of $D_{pp}(r)$ to $D_{1,23}(r)$ is to be done, the net protein-lipid correlation is given by the difference between the correlation of the electrons in the protein with those in the polar region (++) and in the hydrocarbon interior (+−). This is then written as $D_{1,23}(r) = 2\overline{V}_1\rho_p(\overline{V}_2 f^- \rho_1^- + \overline{V}_2 f^+ \rho_1^+)$, where f^- and f^+ are the respective fractions of the two lipid regions; for a head group region 10 Å thick and a boundary to boundary bilayer thickness of 22 Å, $f^+ = 0.385$ and $f^- = 0.615$. Substituting the known values of all the variables gives

$$D_{pp}(r) = 7.25 \times 10^{-4} \text{ and } D_{1,23}(r) = 7.50 \times 10^{-4},$$

and the ratio of these two quantities, −0.96, is used to scale $D_{pp}(r)$ to the units of $D_{1,23}(r)$. This is the $D_{pp}(r)$ curve shown in Fig. 5.

The difference curve $D'_{1,23}(r)$ for the protein-lipid interaction, taking into account the effect of the presence of other proteins, is shown in the bottom curve of Fig. 5. There is a distinct

isolated negative peak at $r \simeq 35$ Å. Two other diffuse bands are apparent at larger distances, but these average out in the Fourier transforms and contribute little to the intensity patterns in the observable range. They are largely artifactual, and in the real systems would appear as broad oscillations around a constant ρ_0^2; the value of ρ_0^2 would increase or decrease, depending on the relative amounts of protein and lipid present. The dashed portion on the right-hand side of the 35-Å peak has been drawn in to show the effective outer limit of $D'_{1,23}(r)$. Formally, this is accomplished by the function $G(z)$ described in the Appendix. Thus the effect of $D_{pp}(r)$ is to limit the correlation range of $D_{1,23}(r)$ to those lipids contained in an annular region of ~50 Å around each protein. Thus $D_{pl}(r)$ in Eq. 9 becomes independent of $1 - x$ and depends only on the protein concentration, as demonstrated by the experimental curves.

Similar curves are obtained for the other two cases, except that the negative peak moves out to larger values of r as the protein takes up a more symmetrical position with respect to the bilayer (not shown).

The intensity profiles of the protein-lipid interaction terms, obtained by Fourier transformation of the $D'_{1,23}(r)$s for the three protein positions are shown in Fig. 6. The curve calculated for the most asymmetrical disposition of the protein, that is, where it protrudes out from one side of the membrane with its other end contiguous with the opposite bilayer surface, gives a curve whose maximum coincides within experimental error with the measured curve and whose width and shape also agree with the data. The curve for the symmetrically placed protein gives two maxima, neither of which is within reasonable agreement with the data. The intermediate case gives a single peak whose maximum occurs at a much smaller value of s than the experimental one, a deviation well beyond experimental error. Thus the asymmetrical position is the only one consistent with the measured curves.

To conclude, it is appropriate to emphasize how the present work demonstrates the utility of liquid diffraction technique and theory when applied to the analysis of membrane scattering patterns. This is particularly true in the determination of protein location, where a straight-

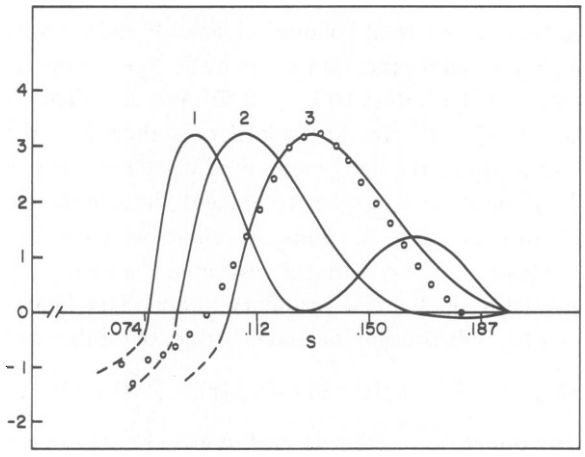

FIGURE 6 Intensity patterns of the protein lipid interaction terms obtained by Fourier transformations of the $D'(r)$ calculated according to Eq. 5. Curves 1 and 3 are for the completely asymmetrical and symmetrical cases, respectively. The points are the experimental data.

forward application of the theory leads to an unambiguous result. This has in the past been one of the most elusive aspects of membrane structure analysis.

APPENDIX

The calculation of the contribution of the protein-lipid correlation to the total intensity is done by first calculating the appropriate distance distribution function $D_{12}(r)$ from a model of a unit of composition (see Theory) and Fourier transforming to obtain the intensity. The geometric model used to calculate

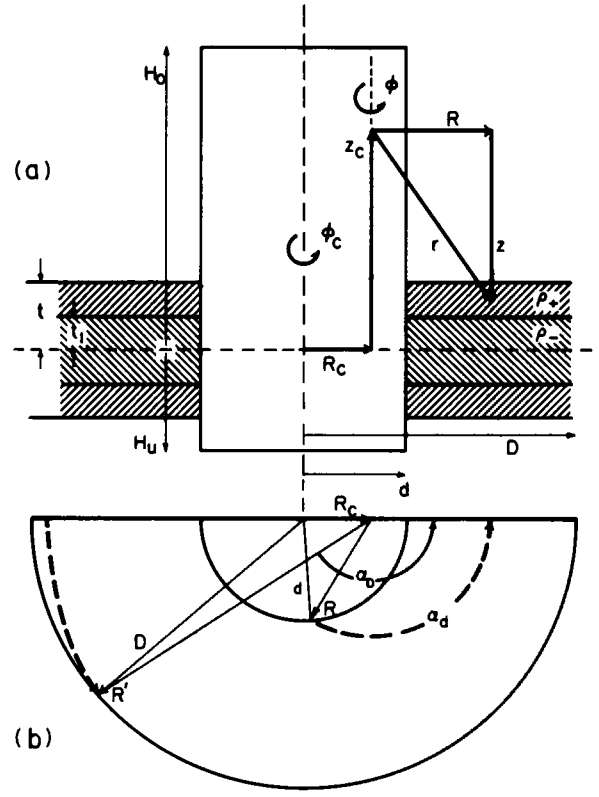

FIGURE A1 (*a*) The cylinder of height $H_0 + H_u$, radius d, and electron density ρ_P traverses an annular lipid bilayer of half-thickness t and radius D. The electron density of the bilayer is approximated by a step function which takes the value ρ_L^+ in the polar region and ρ_L^- in the hydrocarbon region, which has a half-thickness of t_1. A correlation at a distance r is indicated between a point (R_C, z_C, ϕ_C) in the cylinder and a point in the bilayer with coordinate (R, z, ϕ) (taking the first point as the origin). For each r, z, and R are mutually dependent, and we have chosen to integrate with respect to z. The integration with respect to ϕ_C is straightforward, but the limits of integration with respect to ϕ depend on the value of R (Fig. A1 *b*). (*b*) This cross-section of the model taken through the point (R, z, ϕ) in the bilayer shows two examples of paths of integration (dashed arcs) with respect to ϕ at radii R_1 and R_2, from point $(R_C, z_C - z, \phi_C)$. At radius R_1, the path intersects the cylinder at angle α_d. At radius R_2, the path intersects the outer boundary of the annulus at angle $\pi - \alpha_D$. These angles of intersection represent the limits of integration with respect to the variable ϕ in half the plane. Thus, the integration over ϕ yields $2(\alpha_d - \alpha_D)$. However, the angles of intersection depend on the values of R and R_C. In general, $\alpha_d = \arccos[(d^2 - R^2 - R_C^2)/2RR_C]$ when $R < R_C + d$, with a particular value, $\alpha_d = \pi$ when $R \geq R_C + d$. Similarly, $\alpha_D = \arccos[(D^2 - R^2 - R_C^2)/2R\,R_C]$ when $R > D - R_C$, and $\alpha_D = \pi$ when $R \leq D - R_C$.

$D_{12}(r)$, shown in Fig. A1 *a*, is described by cylindrical coordinates. The electron density of the cylinder, ρ_P, is a constant, while the electron density of the bilayer, $\rho_L(z_C - z)$, is a function of the relative coordinate, z. The number of pairs of electrons situated between r and $r + dr$ from each other equals the product of electron densities times the product of volume elements integrated over both the volume of the cylindrical protein and the volume of the lipid annulus surrounding it. Taking advantage of the cylindrical symmetry of the model and expressing the position of the annular volume element with relative coordinates (Fig. A1 *a*) the resulting fivefold integral can be reduced to:

$$D_{12}(r) = 2\pi \int_{-H_u}^{H_0} \int_{A}^{d} \int_{-B_u}^{B_0} \rho_P \rho_L (z_C - z) \cdot 2[\alpha_d(R, R_C) - \alpha_D (R, R_C)]\, R_C R \frac{dR}{dr}\, dz\, dR_C\, dz_C. \quad (A1)$$

For any annulus of inner radius d, and outer radius D, $2\alpha_d(R, R_C)$ is the angle subtended by the intersections of the path of integration in the annulus with the surface of the cylinder; similarly $2\alpha_D(R, R_C)$ is the angle subtended by that part of the path of integration which passes outside the annulus (Fig. A1 *b*). The difference, $2\alpha_d - 2\alpha_D$, is a measure of the number of points lying within the lipid annulus at a radius R. The variable R is not independent, since $R = \sqrt{r^2 - z^2}$; α_D and α_d are functions of z, and $R\, dR/dr = r$. The limits to z, B_u, and B_0 cannot be larger than r; consequently B_u is r or $H_u + t$, whichever is smaller, and B_0 is r or $H_0 + t$, whichever is smaller. The lower limit to R_C, A is 0 or $d - R$, whichever is larger. Inserting

$$g(z) = \int_{-H_u}^{H_0} \rho_P \rho_L (z_C - z) dz_C$$

and

$$F(z) - G(z) = \int_{A}^{d} [\alpha_d(z, R_C) - \alpha_D(z, R_C)] R_C\, dR_C$$

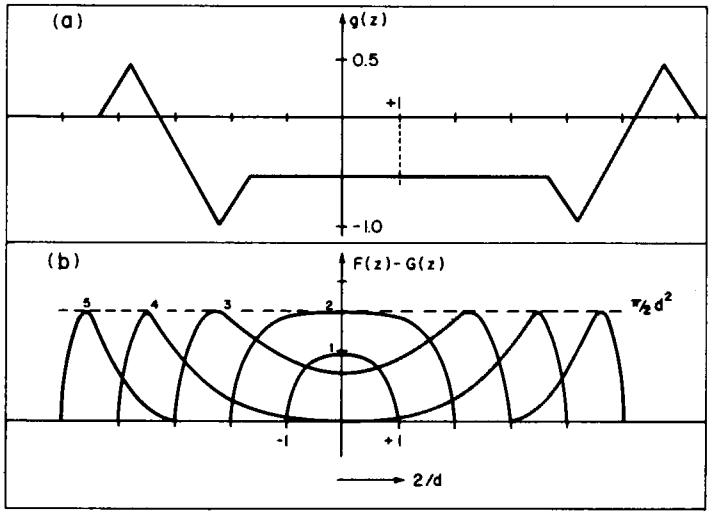

FIGURE A2 (*a*) The function $g(z)$ for a cylinder with an axial ratio of 4, in a bilayer in which the total number of electrons is negative. The units along the abcissa are multiples of the cylinder radius. $g(z)$ has the dimensions electrons/Å^2. In this example, the function is symmetrical about $z = 1$, indicating that the difference $H_0 - H_u = 2d$, a slightly asymmetric arrangement of cylinder and bilayer. (*b*) The function $F(z) - G(z)$ for five values of r. Units along the abcissa are expressed as multiples of d and along the ordinate as multiples of d^2. 1, $r = d$; 2, $r = 2d$; 3, $r = 3d$; 4, $r = 4d$; 5, $r = 5d$.

into Eq. A1 results in a single integral to be evaluated numerically:

$$D_{12}(r) = 4\pi r \int_{-B_u}^{B_0} g(z) \cdot [F(z) - G(z)]dz. \qquad (A2)$$

The values of $g(z)$ (Fig. A2 *a*) are determined by the position of the cylinder ends relative to the center of the bilayer and by the electron density profile of the bilayer. The asymmetry of the placement of the protein in the membrane is described by this function. The difference function $F(z) - G(z)$ describes the inner and outer boundaries of the system with respect to the variable R. The term $F(z)$ is given by

$$F(z) = \pi/2\, d^2\, [1 - \mathcal{L}(R/2d)],$$

and depending on the magnitude of R, takes the value

$$F(z) = \pi/2\, d^2,$$

$$= d^2 \arcsin [(R/2d) + (R/2d)\sqrt{1 - (R/2d)^2}],$$

for $R \geq 2d$ and $R < 2d$, respectively. Here $\pi\mathcal{L}(x)$ is the common area of two circles of unit radius with centers separated by the distance x. For $r \gg D$, $F(z)$ is a nearly rectangular function equal to $\pi/2\, d^2$ inside $z < r$ and equal to zero for $z \geq r$ (Fig. A2 *b*). $F(z)$ represents the interaction with a lipid annulus of radius equal to the largest value of r under consideration (in effect, a sheet of infinite extent). The effect of truncation of the annulus at a radius D is expressed by the term $G(z)$:

$$G(z) = 0 \qquad : R \leq (D - d)$$

$$= \pi/2\, d^2 \qquad : R \geq (D + d)$$

$$= -D^2/2 \arccos\left(\frac{D^2 - d^2 + R^2}{2DR}\right) + d^2/2 \arccos\left(\frac{D^2 - d^2 - R^2}{2dR}\right)$$

$$+ \sqrt{-[R^2 - (D + d)^2][R - (D - d)^2]}/4 \qquad : D - d < R < D + d.$$

The function, $F - G$, is plotted in Fig. A2 *b*. Note that for increasing values of r, $F - G$ is zero in a region of increasing size around the center; consequently, for large r (depending on the asymmetry of the placement of the protein), $D(r)$ must equal zero. The truncation effect in a real system is elaborated on in the Discussion. Copies of a Fortran program for evaluating $D_{12}(r)$ are available on request.

Supported by National Institutes of Health grants GM 23084 to G. W. Brady, AM 8687 to G. Meissner, and GM 24006-03 to R. Spehr.

Received for publication 4 March 1980 and in revised form 26 November 1980.

REFERENCES

1. BEEMAN, W. W., P. KAESBERG, J. W. ANDEREGG, and M. B. WEBB. 1957. Size and shape of particles from small angle x-ray scattering. *Handbuch der Physik.* **32**:321–389.
2. BRADY, G. W., P. S. BIRNBAUM, M. A. MOSCARELLO, and D. PAPAHADJOPOULOS. 1979*a*. Liquid diffraction analysis of the model membrane system, egg lecithin and myelin membrane protein (N-2). *Biophys. J.* **25**:23–42.
3. BRADY, G. W., P. S. BIRNBAUM, and M. A. MOSCARELLO. 1979*b*. The model membrane system egg lecithin and myelin membrane protein (N-2). Effect of solvent density variation on the x-ray scattering. *Biophys. J.* **25**:49–60.
4. BRADY, G. W., D. B. FEIN, and W. A. STEELE. 1977. X-ray scattering from adsorbed xeonon monolayer films. *Phys. Rev.* **15**:1120–1134.
5. CHEN, P. S., T. Y. TORIBARA, and H. WARNER. 1956. Microdetermination of phosphorus. *Anal. Chem.* **28**:1756–1758.

6. DEAMER, D. W., and R. J. BASKIN. 1969. Ultrastructure of sarcoplasmic reticulum preparations. *J. Cell Biol.* **42**:296–307.
7. DUPONT, Y., S. C. HARRISON, and W. HASSELBACH. 1973. Molecular organization in the sarcoplasmic reticulum membrane studied by x-ray diffraction. *Nature (Lond.).* **244**:555–558.
8. GUINIER, A., and G. FOURNET. 1955. Small angle scattering of x-rays. John Wiley & Sons. New York.
9. HERBETTE, L., J. MARQUARDT, A. SCARPA, and J. K. BLASIE. 1977. A direct analysis of lamellar x-ray diffraction from hydrated oriented multilayers of fully functional sarcoplasmic reticulum. *Biophys. J.* **20**:245–272.
10. HIDALGO, C., N. IKEMOTO, and J. GERGELY. 1976. Role of phospholipids in the calcium-dependent ATPase of sarcoplasmic reticulum. Enzymatic and ESR studies with phospholipid replaced membranes. *J. Biol. Chem.* **251**:4224–4232.
11. LEMAIRE, M., K. E. JORGENSEN, H. ROIGAARD-PETERSEN, and J. V. MALLER. 1976. Properties of deoxycholate solubilized sarcoplasmic reticulum Ca^{2+}-ASPase. *Biochemistry.* **15**:5805–5812.
12. LEMAIRE, M., J. M. MOLLER, and C. TANFORD. 1976*b*. Retention of enzyme activity by detergent-solubilized sarcoplasmic Ca^{2+}-ATPase. *Biochemistry.* **15**:2336–2342.
13. LEMAIRE, M., K. E. LIND, K. E. JORGENSEN, H. ROIGAARD, and J. V. MOLLER. 1978. Enzymatically active Ca^{2+}-ATPase from sarcoplasmic reticulum membranes solubilized by nonionic detergents. *J. Biol. Chem.* **253**:7051–7060.
14. LIN, S. C., and C. R. WORTHINGTON. 1974. Electron density levels of sarcoplasmic reticulum membranes. *Arch. Biochem. Biophys.* **163**:332–342.
15. LOWRY, O. H., N. J. ROSEBROUGH, A. L. FARR, and R. J. RANDALL. 1951. Protein measurement with the Folin phenol reagent. *J. Biol. Chem.* **193**:265–275.
16. MACLENNAN, D. H. 1970. Purification and properties of an adenosine triphosphatase from sarcoplasmic reticulum. *J. Biol. Chem.* **245**:4508–4518.
17. MEISSNER, G., and S. FLEISCHER. 1971. Characterization of Sarcoplasmic Reticulum from Skeletal Muscle. *Biochim. Biophys. Acta* **241**:356–378.
18. MEISSNER, G., E. G. CONNER, and S. FLEISCHER. 1973. Isolation of sarcoplasmic reticulum by zonal centrifugation and purification of Ca^{2+}-pump and Ca^{2+}-binding proteins. *Biochim. Biophys. Acta.* **298**:246–269.
19. MEISSNER, G., and S. FLEISCHER. 1972. The role of phospholipid in Ca^{2+}-stimulated ATPase activity of sarcoplasmic reticulum. *Biochim. Biophys. Acta.* **255**:19–23.
20. MEISSNER, G. 1975. Isolation and characterization of two types of sarcoplasmic reticulum vesicles. *Biochim. Biophys. Acta.* **389**:51–68.
21. MOORE, B. M., B. R. LENTZ, and G. MEISSNER. 1978. Effects of sarcoplasmic reticulum Ca^{2+}-ATPase on phospholipid bilayer fluidity. *Biochemistry.* **17**:5248–5255.
22. NAKAMURA, H., R. L. JILKA, R. BOLAND, and A. R. MARTONOSI. 1976.Mechanism of ATP hydrolysis by sarcoplasmic reticulum and the role of phospholipids. *J. Biol. Chem.* **251**:5414–5423.
23. POPE, E. H., W. MENKE, D. WEICK, and R. HOSEMANN. 1974. Small angle x-ray scattering of thylakoid membranes of *Rhodopseudomonas spheroides* in aqueous suspensions. *Biophys. J.* **14**:221–262.
24. ROUSER, G., and S. FLEISCHER. 1967. Isolation, characterization and determination of phospholipids in mitochondria. *Methods Enzymol.* **10**:385–405.
25. SAITO, A., C. WANG. and S. FLEISCHER. Membrane asymmetry and enhanced ultrastructural detail of sarcoplasmic reticulum revealed with the use of tannic acid. *J. Cell Biol.* **79**:601–616.
26. SCALES, D., and G. INESI. 1976. Assembly of ATPase protein in sarcoplasmic reticulum membranes. *Biophys. J.* **16**:735–751.
27. STEWART, P. S., and D. H. MACLENNAN. 1974. Surface particles of sarcoplasmic reticulum membranes. Structural features of the adenosine triphosphatase. *J. Biol. Chem.* **249**:985–993.
28. STUHRMANN, H. B. 1973. Comparison of the three basic scattering functions of myoglobin solution with those from the known structure in crystalline state. *J. Mol. Biol.* **77**:363–369.
29. WILKINS, M. H. F., A. E. BLAUROCK, and D. M. ENGELMAN. 1971. Bilayer structure in membranes. *Nat. New Biol.* **230**:72–76.